



Ordered phases and texture in spray-formed Fe–5 wt%Si

R.D. Cava^a, W.J. Botta^b, C.S. Kiminami^{b,*}, M. Olzon-Dionysio^c, S.D. Souza^c, A.M. Jorge Jr.^b, C. Bolfarini^b

^a Post-Graduate Program in Materials Science and Engineering, Department of Materials Engineering, Federal University of São Carlos, São Carlos, SP, Brazil

^b Department of Materials Engineering, Federal University of São Carlos, São Carlos, SP, Brazil

^c Department of Physics, Federal University of São Carlos, São Carlos, SP, Brazil

ARTICLE INFO

Article history:

Received 1 July 2010

Received in revised form

18 November 2010

Accepted 28 November 2010

Available online 4 December 2010

Keywords:

Fe–Si alloy

Order–disorder reactions

Rolling

Mössbauer spectroscopy

ABSTRACT

Fe–Si alloys have excellent soft magnetic properties, especially around 12 at.% Si. However, their industrial applications are limited because they lack the ductility required in rolling operations for the fabrication of thin sheets, thus leading to cracking. The brittleness of high silicon alloys is caused by order–disorder reactions at low temperatures. This work involved an analysis of the effect of heat treatment on the crystalline structure of thin sheets of Fe–5 wt%Si alloy obtained in a two-step fabrication route: (1) spray forming of Fe–3.5%Si + 2.0%Si_p composite and (2) rolling and heat treatment of the composite to dissolve the silicon and homogenize its content across the thickness of sheet samples. Structural and microstructural analyses indicated the success in fabricating thin sheets of Fe–5 wt%Si alloys with such strategy. The presence of the ordered B2 phase had an important effect on the texture development and therefore on the magnetic properties of these alloys.

© 2010 Elsevier B.V. All rights reserved.

1. Introduction

The addition of silicon to iron improves the latter's magnetic properties by increasing the material's electrical resistivity and decreasing its magnetic anisotropy constant and magnetostriction [1]. However, at concentrations above 3.5 wt%, silicon strongly decreases the ductility of Fe–Si-alloys, rendering the material too brittle to be cold or hot rolled without cracking during the production of thin sheets for electromagnetic applications [2]. Iron-based alloys containing 10–20 at.% Si form two kinds of ordered structures: B2 (*Pm3m*) and DO₃ (*Fm3m*) on the basis of the fundamental crystal lattice of bcc (*Im3m*) [3,4]. Up to about 11 at.% Si, the B2 structure is formed from A2 (disordered solid solution with bcc lattice) by unlike-atom pairing of the first nearest neighbors. A further increase of the silicon content leads to a phase transition towards the ordered DO₃ structure through additional ordering between the second neighboring atoms. Between about 11 and 14.5 at.% both structures can be observed [3,5].

Viala et al. [6] reported that, at cooling rates below 1000 °C/min, the ductile-fragile transition of Fe–6.5 wt%Si occurred by B2 phase ordering, which led to the formation of super-lattice dislocation. Moreover, the magnetic properties of Fe–Si alloys are affected by disorder–order transitions, a dependence that has been investigated by several authors [7,8]. The DO₃ phase has been observed only in low cooling rate processing.

Narita and Enokisono [9] studied the magnetic properties of a Fe + Si6.5 wt% alloy and concluded that the DO₃ ordered structure was more effective in improving the magnetic properties than the B2 ordered phase. However Degauque et al. [10] concluded that losses were lower in the Fe + Si6.5 wt% ribbons (which involved B2 ordered phase) than in those involving DO₃ ordered structure. To explain the origin of this difference, Altoe et al. [11] studied the effect of aging treatments in the temperature range 400–700 °C on the microstructure and the magnetic properties of Fe–6.4 wt%Si. The authors concluded that the existence of 1/4 [1 1 1] antiphase boundaries of B2 showing a marked anisotropy induces a deterioration of the magnetic properties since they lead to a reduced mobility for the magnetic domain walls whereas large grain size and more isotropic B2 antiphase boundaries seem to be promising. In addition, Faudot et al. [12] showed that the DO₃ phase hardens the material whereas the B2 phase softens it.

The literature has reported several successful productions of high Si content Fe–Si thin sheet by carefully controlled forming processes and subsequent rolling operations. Yamaji et al. [13] produced Fe–6.5%Si sheets by CVD technique in the NKK Corporation, in Japan. The thickness ranged from 0.1 to 0.3 mm and the maximum width was 600 mm. However, the manufacturing capacity is limited, the costs for production are very high and it is associated with environmental pollution induced by using SiCl₄. Arai and Tsuya [14] reported the preparation of ribbon-form Fe–Si alloy containing around 6.5% silicon by rapid quenching technique. The ribbon size was 20–150 μm in thickness and 2–25 mm in width. Although the ribbons could be easily cold rolled, the thickness and width were limited and the technique could not satisfy the com-

* Corresponding author.

E-mail addresses: kiminami@ufscar.br, moreira@ufscar.br (C.S. Kiminami).

mercial production. Li et al. [15] tried to produce Fe–6.5 wt%Si alloy by Powder Metallurgy. However, this technique has limited production and there is the necessity of high temperature sintering, which increases the cost of the final product.

To overcome this lack of productivity and volume of the final product, our group has studied and reported the successful productions of high Si content Fe–Si thin sheet by carefully controlled spray forming process and subsequent rolling operations [16–21]. In recent work, Kasama et al. [21] have investigated the disorder/order reaction ($A2 \rightarrow B2 + DO3$) in spray-formed Fe–5 wt%Si–1.5 wt% alloy at warm temperatures and have verified the coexistence of the A2, B2 and DO3 phases in this temperature range. Related with this study, steel makers have recently begun to take an interest in warm (ferritic) rolling, as it has the potential to broaden the product range and decrease the cost of hot-rolled strip. These advantages can affect all stages of the rolling process, beginning with reheating, followed by warm rolling, pickling, and cold rolling [22].

The spray forming process is a variant of rapid solidification processes and is based on the atomization of a liquid metal stream by an inert gas [23]. In this process, the atomized droplets are consolidated into a dense deposit on a substrate. Our group investigated the possibility of keeping the A2-disordered phase metastable at a temperature below 973 K by adding Al to spray-form deposits of Fe–Si alloys, which allowed these deposits to be rolled without cracking [24,25]. However, the addition of aluminum to the alloy is associated with the formation of enhanced inclusions that impair its magnetic properties. Therefore, efforts have focused on the fabrication of an Al-free alloy.

To overcome the lack of ductility, we developed a Fe–5.5 wt%Si alloy as a composite: Fe–3.5%Si + 2%Si_p produced by spray forming. To improve the magnetic properties, the presence of texture after annealing, such as the $\langle 110 \rangle$ /rolling plane, is desirable and in the present work we evaluated the microstructure and the crystallographic texture of the spray formed Fe–3.5 wt%Si + 2 wt%Si_p after rolling and heat treatment for thin sheets production.

2. Experimental procedures

5 kg of commercial Fe–3.5 wt%Si matrix alloy was melted inductively in an alumina crucible and superheated to 1650 °C. The molten alloy was disintegrated into a dispersion of micron-sized droplets using nitrogen at a pressure of 0.80 MPa. Simultaneously, 2 wt% of commercial Si particles, ranging from 106 to 250 μm and with an irregular morphology, was injected into the atomized spray under a nitrogen pressure of 0.20 MPa. The flying distance was approximately 350 mm and the atom-

Table 1
Chemical composition of the matrix alloy and particulate used in this work.

Elements		Fe	Si	C	Ca	Al
wt%	Matrix	Bal.	3.51	0.004	–	–
	Particulate	–	99.4	0.004	0.33	0.08

ized metallic droplets and co-injected particles were deposited onto a 1020 steel substrate rotating at 60 rpm. Fig. 1 resumes this procedure and shows schematics of the equipment [26]. Nitrogen of 99.99% purity was used for the atomization. Table 1 shows the chemical composition of the matrix and particulate used for the composite, determined by SEM-EDS.

Specimens with dimensions of 70 mm × 30 mm × 5.2 mm were machined from the deposit, reheated at 850 °C for 5 min and warm rolled to the final thickness of 0.45 mm, corresponding to a total reduction of 91.3%. The sheet specimens were heat-treated as follows: Heat Treatment (1) (which will be referred as HT1): was made following industrial procedure to produce annealing and grain growth at 780 °C for 6 h and iron oxidation surface treatment for another 2 h at 510 °C (this heat treatment was carried out in the industrial facility of an electrical motor manufacturer); and Heat Treatment (2) (which will be referred as HT2): annealing at 1250 °C for 1 h in vacuum and cooling in air (carried out in laboratory conditions), to increase the grain growth and to evaluate the effect of more isotropic B2 antiphase boundaries in large grain sizes.

The phases and the first evaluation of preferential texture were identified by X-ray diffraction (XRD) using monochromatic Cu-K α radiation with an angular pass of 0.032° in a diffractometer equipped with a C-monochromator. Electron backscattered diffraction (EBSD) analyses were performed in a field emission gun scanning electron microscope (FEG-SEM) equipped with an EBSD system.

Mössbauer experiments for heat-treated materials were performed at room temperature in transmission geometry with a constant acceleration signal employing a ⁵⁷Co(Rh) source. The Mössbauer spectra were analyzed with Normos [27] software, assuming Lorentzian peak shapes. The spectra were fitted employing different interactions, each corresponding to one type of Fe site surrounded by different environments. The fitting parameters, isomer shift (δ) relative to α -Fe, quadrupole splitting (Δ) and hyperfine field (B) were refined separately.

3. Results and discussion

Table 2 shows the Vickers hardness and grain size of rolled and heat-treated samples. These results indicate that despite the high grain growth promoted by HT2, the hardness increased in this condition, showing that HT2 was more effective in dissolving and distributing the silicon particles. The EDS analysis revealed the presence of 4.9 wt% of Si in HT2, while HT1 showed only 3.51 wt%, suggesting some lost of Si in HT1 samples. These results suggest a probable formation of the ordered DO3 and B2 phases, as discussed below.

To confirm the presence of magnetic phases, XRD and EBSD techniques were used. Fig. 2 shows XRD patterns of HT1 and HT2

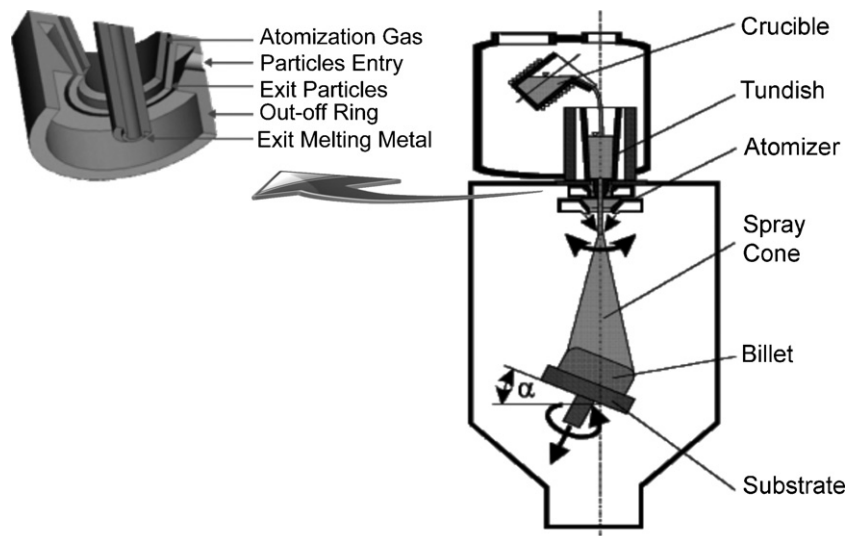


Fig. 1. Schematics of the spray forming equipment and co-injection system [26].

Table 2
Vickers hardness and grain size of rolled and heat-treated samples.

Sample	Hardness (HV _{0.5})			Grain size (μm)		
	Rolled material	Heat Treatment (1)	Heat Treatment (2)	Rolled material	Heat Treatment (1)	Heat Treatment (2)
Mean value	256.60	186.00	203.80	14.70	146.51	361.51
Standard deviation	7.96	6.70	8.10	3.20	27.76	80.27

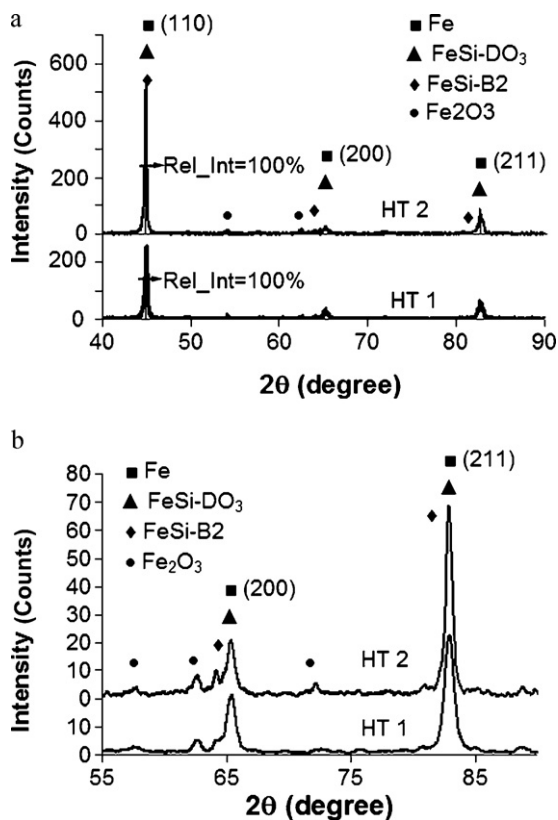


Fig. 2. (a) XRD patterns of HT1 and HT2 compared with the relative intensity of the (110) direction (100%) parallel to the rolling direction. (b) Amplified detail of Fig. 2a, confirming the presence of B2, DO3 and Fe₂O₃ phases.

compared with the relative intensity of the (110) direction (100%) parallel to the rolling direction. The peaks in Fig. 2a were identified as bcc-Fe, B2, DO3 and Fe₂O₃ phases. Fig. 2b is an amplified detail of Fig. 2a, confirming the presence of B2, DO3 and Fe₂O₃ phases. Rietveld analyses indicated that the quantities of B2 phase is 62% larger in sample HT2 than in sample HT1, while the amount of Fe₂O₃ is almost the same in both samples. It is important to note that in both samples a strong texture can be observed ($\langle 110 \rangle$ //rolling direction); however, in the HT2 sample this texture was about 5 times the relative intensity for the 100% peak and only 1.8 times was observed in sample HT1. As mentioned before, this preferred orientation can improve the magnetic properties.

Table 3
Mössbauer parameters of composite alloy heat-treated in two conditions.

Structure	Heat Treatment (1)				Heat Treatment (2)			
	B [T]	δ [mm/s]	Δ [mm/s]	Area [%]	B [T]	δ [mm/s]	Δ [mm/s]	Area [%]
S1	33.0	0.013	0.00	31	32.90	0.01	0	45.66
S2	31.4	0.020	0.027	38	29.62	0.03	0.04	16.53
S3	30.4	0.060	-0.01	25	30.62	0.06	-0.01	33.70
S4	27.2	0.10	0.02	3	27.08	0.10	0.02	1.35
S5	0.00	0.042	1.63	2	0.00	0.03	1.53	2.75
S6	19.6	0.25	0.02	0.00	19.60	0.25	0.02	0.00

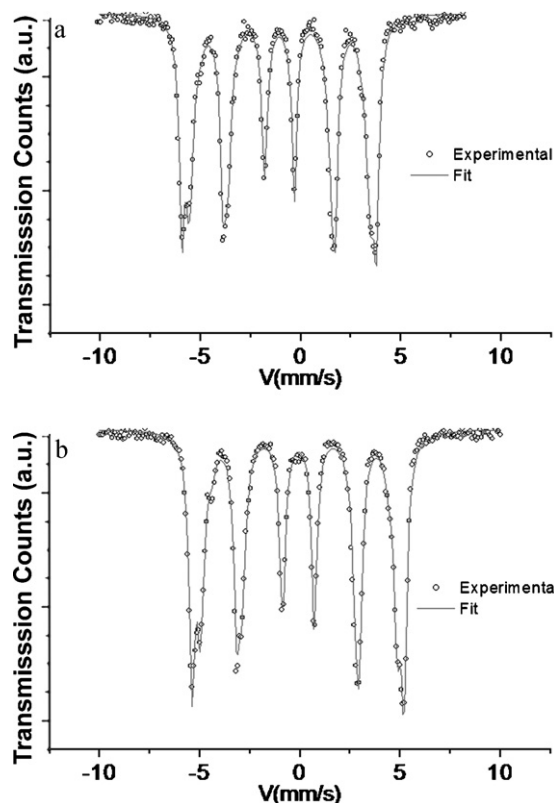


Fig. 3. Mössbauer transmission spectra of (a) Heat Treatment (1), and (b) Heat Treatment (2).

Due to XRD peak overlapping, the presence of the DO3 phase was analyzed by Mössbauer measurements. Fig. 3 shows the Mössbauer spectra for the heat-treated alloys. The fitting parameters (δ , relative to α -Fe, Δ and B) and the relative area of the different Fe sites are shown in Table 3. The Mössbauer spectra showed two structures: a bcc-Fe with a hyperfine field of $B = 33$ T and Fe–Si with a Fe₃Si DO3 structure. In the latter structure, the hyperfine splitting was 3% lower than the reference value [28], probably due to the effect of larger grain size. A comparison of these results with recent findings [25] indicates that the area of the bcc-Fe structure increased from 24% [23] to 32% (HT1) and 42% (HT2), while the DO3 structure decreases from 76% [23] to 66% (HT1) and 55% (HT2) and the S6 structure was absent from the two alloys studied

here. Also, from the six possible sub-spectra observed for DO3 [28] only three [$B = 31.4, 30.4, 27.2 \text{ T}$] were present in this study and the doublet observed in small percentage (2% and 3%) is possibly due to some oxide formed during the sample preparation. The presence of A2 and B2-structures were not clear. Certainly, A2 is not present because it was not observed in XRD analysis but the non-identification of B2 could be due to the small amount, as already pointed out in the XRD analysis. In addition, one can infer from these changes in DO3 findings that a larger amount of B2 was probably formed during the disorder/order reaction ($A2 \rightarrow B2 + DO3$) inducing the HT2 sample to acquire stronger preferential orientation.

Fig. 4 shows TEM dark field images taken using a $[200]$ B2 superlattice reflection and $[001]$ diffraction pattern for both samples, in (a) for HT1 and in (b) for HT2. The formation of B2 was not sup-

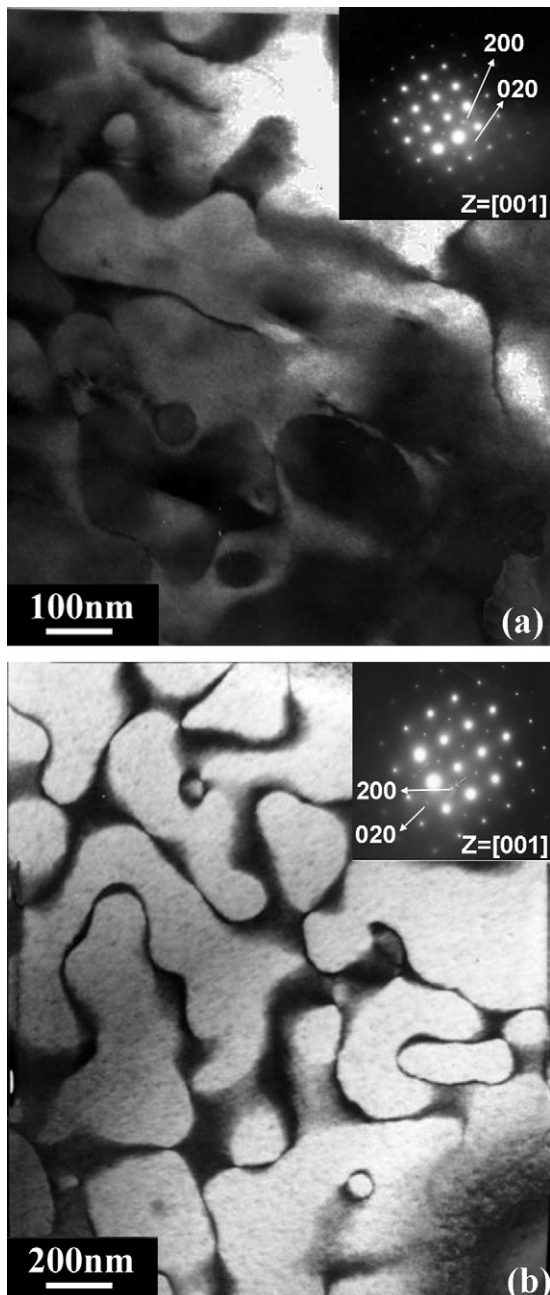


Fig. 4. TEM dark field images taken using a $[200]$ B2 superlattice reflection and $[001]$ diffraction pattern for both samples, in (a) for HT1 and in (b) for HT2.

pressed in both samples; it is also important to note that for HT2 the B2 domain structure is well developed and the B2 antiphase domain size is in the range of 100–300 nm. For HT1 the B2 domain structure is very diffuse indicating that the lower treatment temperature, that resulted in reduced grain growth, did not lead to a complete transformation as occurred for sample HT1. As observed in other studies [10] phase ordering is a non-negligible parameter for the magnetic properties and a well-developed B2 domain contributes to increase these properties.

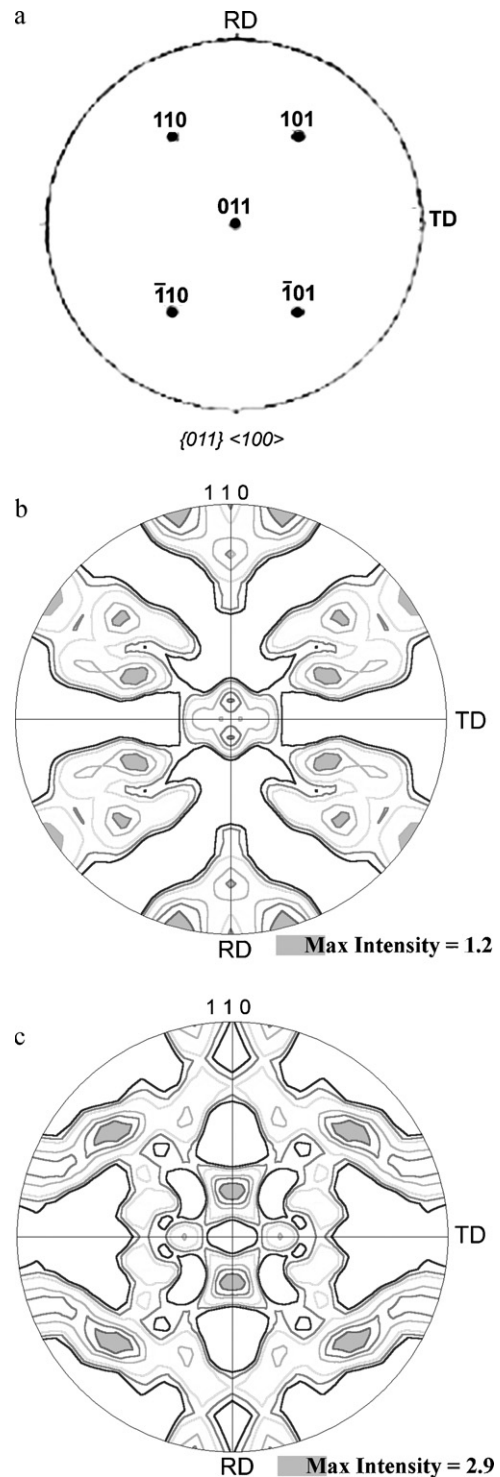


Fig. 5. (a) Reference system used to analyze the pole figures. (b) Pole figure of the EBSD plots obtained for HT1. (c) Pole figure of the EBSD plots obtained for HT2.

Fig. 5 shows the EBSD plots of pole figures for the reference system used to analyze the pole figures in (a) and the pole figures obtained for both samples: in (b) for HT1 and in (c) for HT2. Fig. 5a shows the 0 1 1 pole figure, one of the poles is oriented parallel to the Normal Direction of the rolling plane (ND) (center of the pole figure) but the other ones will be at 60° or 90° angles but tilted 45° from the rolling direction (RD), and, in this case, the (0 1 1) plane is oriented towards the ND and the [0 0 1] inside the (0 1 1) plane is along the RD. Fig. 5b and c shows that sample HT2 acquired better preferential orientation than that for HT1. For HT2 the microtexture is preferentially the Goss ($\langle 110 \rangle$ //rolling direction) while in HT1 we only see a tendency to form such preferential orientation.

The best results, concerning preferential orientation, are ascribed to the higher silicon content and to the recrystallized-coarsen grain size present in sample HT2. The antiphase boundaries of ordered B2 and the grain size seems to play a role in the preferential orientation (consequently in the magnetic properties) of these alloys and could be responsible for the high difference in the texture results for the HT2. In fact, the antiphase boundaries of B2 with a marked anisotropy, as observed in sample HT1, can result in poor preferential texture due to the reduced interphase mobility whereas large grain size and more isotropic B2 antiphase boundaries seem to be promising for the texture development.

4. Conclusions

- The production of a composite material by co-injection of silicon particles into a Fe–Si spray allowed the fabrication of thin sheets of Fe–Si alloys with higher Si content than that found in commercial alloys.
- Heat Treatment at a high temperature (1250 °C) under vacuum was efficient to promote grain growth and silicon dissolution and homogenization throughout the thickness of the sheets.
- The structural characterization of these alloys showed only the presence of the ordered DO3 and B2 phases.
- The antiphase boundaries of ordered B2 and the grain size seems to play a role in the preferential orientation (consequently in the magnetic properties) of these alloys and could be responsible for the high difference in the texture observed for HT2 condition.
- The antiphase boundaries of B2 with a marked anisotropy, as observed in sample HT1, can result in poor preferential texture

due to the reduced interphase mobility whereas large grain size and more isotropic B2 antiphase boundaries seem to be promising for the texture development.

References

- [1] R.M. Bozorth, *Ferromagnetism: Iron-Silicon Alloys*, Van Nostrand, New York, 1993, pp. 67–101.
- [2] Y. Takada, M. Abe, S. Masuda, J. Inagaki, *J. Appl. Phys.* 6410 (1988) 5367–5369.
- [3] S. Matsumura, Y. Tanaka, Y. Koga, K. Oki, *Mater. Sci. Eng. A* 312 (2001) 284.
- [4] P.R. Swann, L. Granás, B. Lehtinen, *Met. Sci.* 9 (1975) 90.
- [5] R.S. Turtelli, R. Grössinger, E. De Morais, V.H. Duong, G. Wiesinger, M. Dahlgren, E. Ferrara, *J. Magn. Mater.* 177/181 (1998) 1389.
- [6] B. Viala, J. Degauque, M. Fagot, M. Baricco, E. Ferrara, F. Fiorillo, *M. Sci. Eng. A212* (1996) 62–68.
- [7] D. Bouchara, M. Agot, J. Degauque, J. Bras, *JMMM* 83 (1990) 377–382.
- [8] J. Degauque, et al., *IEEE Trans. Magn.* 26 (1990) 274–280.
- [9] R. Narita, M. Enokisono, *IEEE Trans. Magn.* 15 (1979) 911.
- [10] J. Degauque, D. Bouchara, M. Fagot, T. Bras, J.P. Redoules, P.H. Chommel, B. Astie, *IEEE Trans. Magn.* 26 (1990) 2220–2222.
- [11] M.V.P. Altoe, M.S. Lancarotte, R. Cohen, F.P. Missell, W.A. Monteiro, J. Degauque, M. Fagot, *IEEE Trans. Magn.* 27 (6) (1991) 5325–5327.
- [12] F. Faudot, J.F. Riallandand, J. Bigot, *Phys. Scr.* 39 (1989) 263–267.
- [13] T. Yamaji, M. Abe, Y. Takada, K. Okada, T. Hiratani, *J. Magn. Mater.* 133 (1994) 187–189.
- [14] K.-I. Arai, N. Tsuya, *IEEE Trans. Magn.* 16 (1) (1980) 126–129.
- [15] Ran Li, Qiang Shen, Lianmeng Zhang, Tao Zhang, *J. Magn. Mater.* 281 (2–3) (2004) 135–139.
- [16] M.C.A. Silva, C. Bolfarini, C.S. Kiminami, *Mat. Sci. Forum* 498 (2005) 111–118.
- [17] C. Bolfarini, A.H. Kasama, R. Machado, A.R. Yavari, G. Vaughan, C.S. Kiminami, W.J. Botta, *J. Metast. Nanocryst. Mater* 20 (21) (2004) 553–556.
- [18] C. Bolfarini, V.S. Leal, W.M. Silva, C.S. Kiminami, *Mat. Sci. Forum* 416/441 (2003) 431–436.
- [19] M.C.A. Silva, C. Bolfarini, C.S. Kiminami, M.J. Kaufman, R. Machado, *Key Eng. Mater.* 191 (2001) 643–648.
- [20] A. Florio Filho, C. Bolfarini, C.S. Kiminami, M.J. Kaufman, *Key Eng. Mater.* 189 (2001) 461–466.
- [21] A.H. Kasama, R. Machado, A.R. Yavari, G. Vaughan, C. Bolfarini, C.S. Kiminami, W.J.F. Botta, *J. Metastable Nanocryst. Mater.* 20–21 (2004) 553.
- [22] J.J. Jonas, *J. Mater. Process. Technol.* 117 (2001) 293.
- [23] A.R. Singer, *Int. J. Powder Metall.* 21 (1985) 219–234.
- [24] A.H. Kasama, R. Machado, A.M. Jorge Junior, W.J. Botta, C.S. Kiminami, C. Bolfarini, *M. Sci. Eng. A* 449 (2007) 375–377.
- [25] C. Bolfarini, F. Audebert, W.J. Botta, C.S. Kiminami, F. Saporiti, A.H. Kasama, B. Arcondo, *Mat. Sci. Forum* 570 (2008) 150–154.
- [26] R.J. Santos, C. Bolfarini, C.S. Kiminami, *Mat. Sci. Forum* 299–300 (1999) 398–406.
- [27] R. Brand, Normos Program, Internal Report, Angewandte Physik, Universität Duisburg, 1987.
- [28] G. Riexckerter, P. Schaaf, Y. Gonsert, *J. Phys. Condens. Matter.* 4 (1992) 295–298.